Incorporation of a Frequency-Dependent Dielectric Response for the Barrier Material in the Josephson Junction Circuit Model

Lei Yu, Nathan Newman, John M. Rowell, and Theodore Van Duzer, *Life Fellow*

***Abstract*—We extend the resistively shunted Josephson (RSJ) junction circuit model originally proposed by Stewart and McCumber to incorporate a frequency-dependent dielectric response so that the influence of free carriers in the barriers can be taken into account. The methodology that we have developed uses an iterative numerical technique to calculate the current–voltage (*I–V*) characteristics of a Josephson junction with a barrier exhibiting both dissipation and dispersion. We give detailed results for two barrier materials with conductivities near the metal–insulator transition: a conventional semiconductor with a relatively high mobility and a strongly scattered defect solid. We show that the incorporation of the dynamic response of free carriers in the barriers of superconductor-normal-superconductor (SNS) junctions significantly influences the dc *I–V* characteristics for the case of material near the metal–insulator transition with high mobility. Hysteretic anomalies occur at nonzero voltages in the *I–V* characteristics associated with the barrier layer's plasma frequency. The resulting features, which we call critical regions, occur when the dc junction voltage $\langle V \rangle$ is equal to $\hbar/2en\sqrt{\tilde{\omega}_p^2 - \Gamma^2}$, where $\tilde{\omega}_p$ is the barrier's plasma frequency, Γ is the quasi-particle scattering rate, n is an integer, and $\hbar$ is the reduced Planck's constant. We also show that our results for SNS junctions with a low-mobility barrier material are essentially identical to the predictions of the simpler RSJ model. Since the method we develope can solve the nonlinear junction equations for a barrier with an arbitrary complex conductivity, it is also capable of including other relevant processes within the barrier, including the influence of excitation from shallow defects or very soft phonon modes, as well as boundary resistances.**

***Index Terms*—Circuit modeling, Josephson junctions, nonlinear equations, superconductor-normal-superconductor (SNS) devices.**

I. Introduction

THE resistively shunted junction (RSJ) model first proposed by McCumber [1], [2] and Stewart [3] is widely used to calculate the current–voltage (*I–V*) characteristics of Josephson junctions. The RSJ model of the junction contains a capacitor C, a resistor R, and a current source. The current source represents the Josephson current $I_c \sin\phi$, where I_c is the maximum critical current of the junction and ϕ is the gauge-invariant phase difference across the junction. The shape of the junction's dc *I–V* characteristics [solid curves in Fig. 1(a)] depends only on the parameter $\beta_C = (2e/\hbar)CI_cR^2$, where e is the electron charge and $\hbar$ is the reduced Planck's constant. The β_C of a junction can be determined by equating the amount of hysterisis in the measured *I–V* characteristics with the theoretical results in Fig. 1(b).

The RSJ model is commonly used to model both superconductor–insulator–superconductor (SIS) junctions with externally shunted resistances and superconductor-normal-superconductor (SNS) junctions [1]–[4]. It is not clear if this model can accurately simulate the latter structures since it does not include the influence of the frequency-dependent response of the barrier. In this paper, we show that a frequency-dependent model of the barrier layer must be included to accurately calculate the dc *I–V* properties of junctions containing a high-mobility barrier material, while the simpler RSJ model may be adequate for SNS junctions with a low-mobility barrier material. First, we describe a formalism to solve the nonlinear Josephson circuit model equation with a complex frequency-dependent conductivity. The response is presented, along with the Fourier components, to provide additional insight into the details of the junction dynamics. Then, we focus our calculation on the case when free carriers dominate the dielectric response of the barrier. The methodology that we have developed uses an iterative numerical technique to calculate the *I–V* characteristics of a Josephson junction with a barrier exhibiting both dissipation and dispersion. We present several examples and focus on those with resistivities near the metal–insulator transition, since it is anticipated that optimized junctions for applications of the dominant digital family will have barriers tuned to near this value. We will explain the basis for this conjecture later in this section. Simulations of the properties of junctions with two different types of barriers tuned to near the metal–insulator transition are presented: a conventional semiconductor with a relatively high mobility and a strongly scattered defect solid. We use parameters from Si for the first case. Our intent in the latter case is to simulate the properties of a Ta_xN-barrier junction, since this device has received considerable attention lately [5]. However, since the relevant material properties of Ta_xN are not yet well established, we use model parameters characteristic of a prototypical strongly scattered defect solid.

For practical applications, there has been renewed interest in the fabrication of self-shunted junctions for rapid single flux

Manuscript received February 21, 2005; revised June 13, 2005. This paper was recommended by Associate Editor M. Mueck. This work was supported in part by the Office of Naval Research under Contract N00014-01-1-0047 and by the University of California, Berkeley, under Contract N00014-00-1-0003.

L. Yu is with the Department of Electrical Engineering, Arizona State University, Tempe, AZ 85287-6006 USA (e-mail: Lei.Yu@asu.edu).

N. Newman and J. M. Rowell are with the Department of Chemical and Materials Engineering, Arizona State University, Tempe, AZ 85287-6006 USA (e-mail: Nathan.Newman@asu.edu).

T. Van Duzer is with the Department of Electrical Engineering and Computer Science, University of California at Berkeley, Berkeley, CA 94720-1770 USA.

Digital Object Identifier 10.1109/TASC.2005.854302

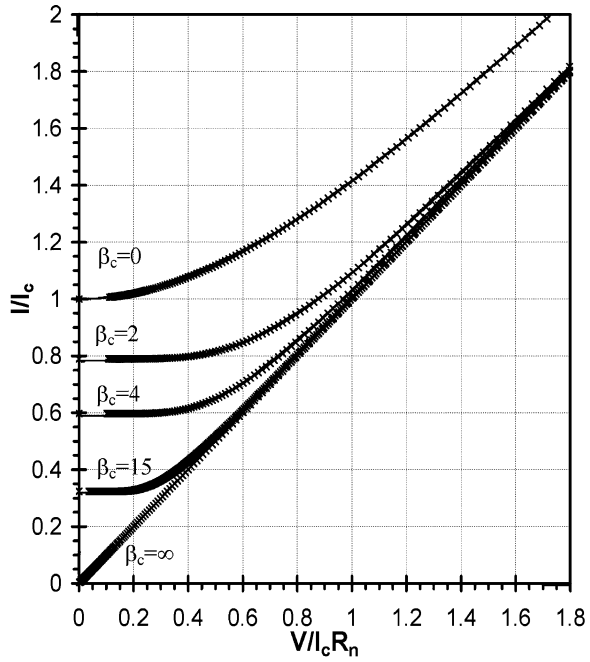

(a)

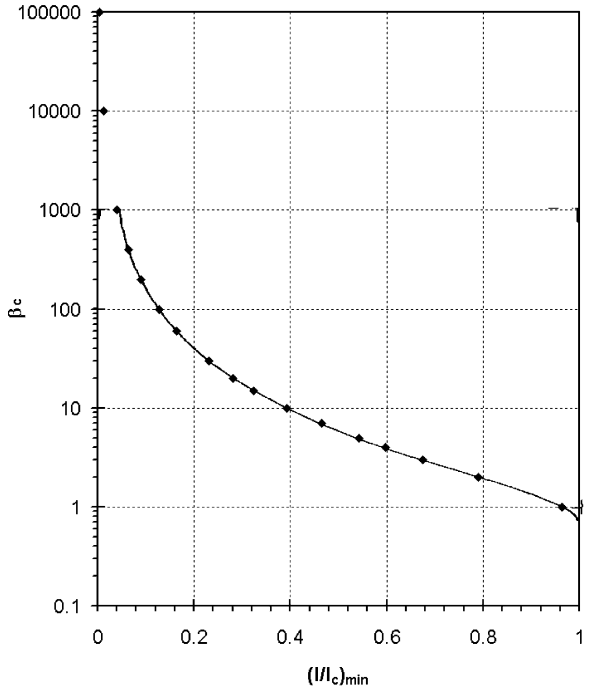

(b)

Fig. 1. (a) Calculated *I–V* characteristics using our methodology for $g_n = 1$ and $h_n = n\kappa\beta_C$ (black crosses) are directly compared with those from McCumber's paper (solid lines). (b) $(I/I_c)_{\min}$ (where $(I/I_c)_{\min}$ is the minimum of I/I_c that is found when it is ramped from values greater than I_c) as a function of β_C for the case $g_n = 1$ and $h_n = n\kappa\beta_C$. Results of our theoretical methodology (black diamonds) are directly compared to those from McCumber's paper (solid lines). In both cases, agreement is excellent.

quantum (RSFQ) logic to facilitate increased density and reduced parasitic inductance over the currently used externally shunted SIS junctions made by the Nb–AlO_x trilayer process. The self-shunted approach uses resistive material as the barrier of the Josephson junction, in the form of an SNS junction (the "N" barrier is a "normal conductor" and can be a metal, semimetal, or doped semiconductor). Tunneling is generally not present in such junctions, supercurrent flows through the normal barrier by a proximity effect and transport of unpaired carriers provides the internal shunt resistor. In the case of barriers with a small free carrier concentration (say$< 10^{21}/\text{cm}^3$) and with a work function difference between the barrier and the electrodes, there can exist a potential barrier at the interface that is depleted (or partially depleted) of carriers, as a result of the formation of a Schottky contact. If this occurs and extends over a distance greater than a few atomic layers (say > 0.5 nm), the barrier will be inhomogeneous and will form a SINIS-like structure. Also, since the barrier thickness can be on the order of or smaller than the average spacing between dopants in a semiconductor, an additional complication can arise from the presence of the lateral potential variations resulting from the discrete dopants. In this work, we will not address such complicated cases and will focus on the modeling of junctions assuming a homogeneous barrier.

The traditional view of SNS junctions is that R_n and I_cR_n are too low to be useful. For example, the high carrier concentration in Cu makes R_n low and depresses I_cR_n as a result of the reduction in the superconducting pair potential at the superconductor/Cu interfaces [6]. However, I_cR_n is not always low in SNS junctions. In work performed about 30 years ago, Van Duzer and his colleagues [7] showed that junctions using a thin membrane of heavily doped silicon as a barrier had I_cR_n values that were a significant fraction of the energy gap. Recently, SNS junctions of the type NbN–Ta_xN–NbN have been shown to have I_cR_n values in excess of 500 μV [5]. The widely used Nb–AlO_x–Nb tunnel junctions have intrinsic I_cR_n product of 2.4 mV [8]. In the current 3-μm line width Nb–AlO_x–Nb tunnel junction process, external shunting limits the effective I_cR_n product to only about 250 μV [8]. Thus, there are strong incentives for adapting the NbN–Ta_xN–NbN junction for the next generations of RSFQ circuit processes.

To make useful SNS junctions for RSFQ circuits, the electrical resistivity of the barrier needs to be accurately controlled to a value near the metal–insulator transition for the following practical reasons. To avoid bit errors caused by noise in 4-K operation, the critical current I_c needs to be at least $\sim$100 μA. To attain a voltage pulse of sufficiently short duration with this logic family, I_cR_n should be 500 μV or higher. It is anticipated that the next generation of superconducting electronics will have line widths of $\sim$1 μm (probably 1.5 μm and then 0.8 μm). Hence, the junction resistance R_n will have to be a few ohms (say 5 Ω). Assuming a material that gives these I_c and R_n values for a layer thickness of 25–100 nm (as is already the case for Ta_xN [5]), then the resistivity implied for this N barrier material will be $\sim$5–20 m$\Omega \cdot$ cm. These values fall in the range in which materials undergo the metal–insulator transition. The use of such a thick barrier also implies that the junction capacitance might be lower than found in the current trilayer process, depending on the effective dielectric constant of the barrier material. This would also improve RSFQ circuit performance as the I_cR_n product scales with $C^{-1/2}$ for fixed values of β_C and J_c. Typically, RSFQ circuit applications require nearly critically damped (i.e., $\beta_C \approx$1 to 2) junctions.

II. Modeling Method

In our model, we assume uniform current across the junction, as occurs at zero magnetic field and in structures that have dimensions small compared to the Josephson penetration depth $\lambda_J = \sqrt{\hbar A/(2eI_c\mu_0(2\lambda+d))}$, where A is the area of the junction, d is the width, and λ is the superconducting electrode's penetration depth. Within these constraints, the electrical properties of Josephson junctions with barriers exhibiting a frequency-dependent dielectric response are simulated.

Following the approach first described by McCumber [1] and Stewart [3], the total current I_T through a Josephson junction can be expressed as the sum of a Cooper pair current I_S and a normal state current I_N. The time dependence of these parameters is implicit and is not included in the notation

$$I_T = I_S + I_N.$$

Using the Josephson current relation, the Cooper pair current is given by

$$I_S = I_c \sin(\phi)$$

where I_c is an input parameter for our model. Values for this parameter can be obtained experimentally or predicted from theoretical work, such as that of Likharev [9], Kupriyanov and Lukichev [18], and/or Devayatov and Kupriyanov [19].

When a junction is dc current biased at a constant value greater than I_c, the voltage in steady state is periodic and can therefore be written in a Fourier series with a fundamental frequency ω_F [4]. The resulting voltage can be expressed by the following Fourier expansion:

$$\begin{aligned} V(t) &= a_0 + \sum_{n=1}^{\infty} \left[a_n \cos(n\omega_F t) + b_n \sin(n\omega_F t)\right] \\ &= a_0 + \sum_{n=1}^{\infty} \left[\alpha_n e^{in\omega_F t} + \alpha_n^* e^{-in\omega_F t}\right] \end{aligned} \quad (1)$$

where

$$\alpha_n = \frac{a_n}{2} - i\frac{b_n}{2}.$$

It is important to note that in solving the traditional RSJ model, the junction bias current is the input variable and the voltage is determined from numerical solution of a nonlinear differential equation. In order to include the frequency-dependent response of the barrier, we used the junction voltage as the input parameter and solved for the bias current. According to linear response theory, homogenous barrier materials have complex dielectric functions, conventionally denoted by $\varepsilon(\omega)$, in which the real component represents conventional dielectric dispersion and the imaginary component dissipation. The actual overall dielectric function $\varepsilon(\omega)$ includes the intraband transitions, free carrier response, and interband transitions. The real and imaginary components are related by the Kramers–Kronig equations as a result of causality.

To find the current, the conductance of the barrier can be expressed using the frequency-dependent complex dielectric function

$$G(\omega) = i\omega\varepsilon_0\varepsilon(\omega)\frac{A}{d} = G_r(\omega) + iG_i(\omega).$$

We assume a "parallel plate" geometry of electrodes and barrier in our analysis. Since the junction width is small compared with the electromagnetic wavelength for the frequencies of our interest, the fields can be considered independent of position in the junction.

The corresponding relationship between the normal state current I_N and voltage $V(t)$ can be mapped into an equivalent linear circuit and can therefore be expressed by the following Fourier sum:

$$I_N = G(0)a_0 + \sum_{n=1}^{\infty} \left[\alpha_n G(n\omega_F) e^{in\omega_F t} + \alpha_n^* G(-n\omega_F) e^{-in\omega_F t}\right].$$

Using (1), and the fact that $\varepsilon(-\omega) = \varepsilon^*(\omega) \Rightarrow G(-\omega) = G^*(\omega)$ [10], the following expression for the normal state current is derived:

$$\begin{aligned} I_N &= G_r(0)a_0 \\ &\quad + \sum_{n=1}^{\infty} \left\{ \begin{array}{l} \left(\frac{a_n}{2} - i\frac{b_n}{2}\right)\left(G_r(n\omega_F) + iG_i(n\omega_F)\right) \\ \quad \times \left[\cos(n\omega_F t) + i\sin(n\omega_F t)\right] \\ + \left(\frac{a_n}{2} + i\frac{b_n}{2}\right)\left(G_r(-n\omega_F) + iG_i(-n\omega_F)\right) \\ \quad \times \left[\cos(n\omega_F t) - i\sin(n\omega_F t)\right] \end{array} \right\} \\ &= G_r(0)a_0 \\ &\quad + \sum_{n=1}^{\infty} \left\{ \begin{array}{l} \left(\frac{a_n}{2} - i\frac{b_n}{2}\right)\left(G_r(n\omega_F) + iG_i(n\omega_F)\right) \\ \quad \times \left[\cos(n\omega_F t) + i\sin(n\omega_F t)\right] \\ + \left(\frac{a_n}{2} + i\frac{b_n}{2}\right)\left(G_r(n\omega_F) - iG_i(n\omega_F)\right) \\ \quad \times \left[\cos(n\omega_F t) - i\sin(n\omega_F t)\right] \end{array} \right\}. \end{aligned}$$

Algebraic manipulation allows us to shorten the expression for the normal state current to

$$\begin{aligned} I_N = G_r(0)a_0 &+ \sum_{n=1}^{\infty} G_r(n\omega_F)\left[a_n \cos(n\omega_F t) + b_n \sin(n\omega_F t)\right] \\ &+ \sum_{n=1}^{\infty} G_i(n\omega_F)\left[b_n \cos(n\omega_F t) - a_n \sin(n\omega_F t)\right]. \end{aligned}$$

Thus, the total current of a Josephson junction is

$$\begin{aligned} I_T &= I_c \sin(\phi) + G_r(0)a_0 \\ &\quad + \sum_{n=1}^{\infty} G_r(n\omega_F)\left[a_n \cos(n\omega_F t) + b_n \sin(n\omega_F t)\right] \\ &\quad + \sum_{n=1}^{\infty} G_i(n\omega_F)\left[b_n \cos(n\omega_F t) - a_n \sin(n\omega_F t)\right]. \end{aligned} \quad (2)$$

This relationship can be mapped into a nonlinear circuit that we will solve for an arbitrary $G(\omega)$ using a numerical technique.

First, we perform the same change of variables used in the RSJ model [1], [4]. Let $r = I_T/I_c$, $\theta = \omega_C t$, $\kappa = \omega_F/\omega_C$, and $\gamma = V/I_c R_0$, where $\omega_C = (2e/\hbar)I_c R_0$ is the Josephson frequency and $R_0 = 1/G_r(0)$ is the dc quasi-particle resistance. Here, r and γ are the normalized current and normalized voltage for the junction, respectively.

Notice that

$$\gamma = \frac{a_0}{I_c R_0} + \sum_{n=1}^{\infty}\left[\frac{a_n}{I_c R_0}\cos(n\omega_F t) + \frac{b_n}{I_c R_0}\sin(n\omega_F t)\right]$$
$$= A_0 + \sum_{n=1}^{\infty}\left[A_n\cos(n\kappa\theta) + B_n\sin(n\kappa\theta)\right]$$

and

$$\frac{d\phi}{d\theta} = \frac{d\phi}{dt}\frac{dt}{d\theta} = \frac{2e}{\hbar}V\frac{1}{\omega_C} = \gamma$$
$$A_n = \frac{a_n}{I_c R_0}, \quad B_n = \frac{b_n}{I_c R_0}$$
$$\phi = \phi_0 + A_0\theta + \sum_{n=1}^{\infty}\left[\frac{A_n}{n\kappa}\sin(n\kappa\theta) - \frac{B_n}{n\kappa}\cos(n\kappa\theta)\right]. \quad (3)$$

After the change of variables, (2) can be rewritten as

$$r = \sin(\phi) + A_0 + \sum_{n=1}^{\infty} G_r(n\kappa\omega_C)R_0\left[A_n\cos(n\kappa\theta) + B_n\sin(n\kappa\theta)\right] + \sum_{n=1}^{\infty} G_i(n\kappa\omega_C)R_0\left[B_n\cos(n\kappa\theta) - A_n\sin(n\kappa\theta)\right].$$

If we set $g_n = G_r(n\kappa\omega_C)R_0$ and $h_n = G_i(n\kappa\omega_C)R_0$, then

$$r = \sin(\phi) + A_0 + \sum_{n=1}^{\infty} g_n\left[A_n\cos(n\kappa\theta) + B_n\sin(n\kappa\theta)\right] + \sum_{n=1}^{\infty} h_n\left[B_n\cos(n\kappa\theta) - A_n\sin(n\kappa\theta)\right]. \quad (4)$$

In Appendix 1, we have shown that the normalized constant supply current r approaches κ, allowing us to equate

$$A_0 = \kappa. \quad (5)$$

Let $\langle X\rangle$ denote the average of X over a full period, that is $\langle X\rangle = (\kappa/2\pi)\int_{\theta=0}^{2\pi/\kappa} X d\theta = (\omega_F/2\pi)\int_{\theta=0}^{2\pi/\omega_F} X dt$. Given the definition of $\omega_C = (2e/\hbar)I_c R_0$, (5) is equivalent to $2e\langle V\rangle = \hbar\omega_F$. The latter equality implies the average voltage is directly proportional to the fundamental frequency of the voltage–current oscillation. This is analogous to the ac Josephson effect, where the dc bias voltage is proportional to the frequency of the current oscillation. Note that the relationship for average voltage is not generally true for a nonperiodic time-varying signal. It is, however, valid in the case of current biased junction circuit in steady state.

The *I–V* curve of a junction can then be reduced to the relationship between the normalized current r and normalized average voltage $A_0 = \langle\gamma\rangle$. With (4) and (5), the task of calculating the *I–V* characteristic now entails finding the functional relationship between r and κ. Appendix 2 describes the iterative algorithm that we use to obtain r as a function of κ and from that the junction *I–V* characteristics.

In the above model, the *I–V* characteristic of the junction is determined solely by I_c and the coefficients g_n and h_n in (4). The parameters $g_n s$ and $h_n s$ depend only on the barrier material's dielectric function and device geometry. Thus, the use of an accurate dielectric function of the barrier material at the dominant harmonics of the Josephson frequency is critical to this model. To avoid the additional complication of selecting appropriate values, in most circumstances we have chosen to use a model frequency-dependent dielectric response that includes only the static dielectric response and that from free carriers. The method we describe here can also be used to simulate junctions using detailed first principles or experimentally derived dielectric data as we have done for this particular case of the Ta_xN barrier.

For conductive barrier junctions, the dielectric function can be dominated by the contribution from the free carriers at the harmonics of the Josephson frequency. Under such circumstances, one can model the response using the following equation for the frequency-dependent dielectric function [10]:

$$\varepsilon(\omega) = \varepsilon_r\left(1 - \frac{\widetilde{\omega}_p^2}{\omega^2 - i\omega\Gamma}\right) = \varepsilon_r\left[1 - \frac{\widetilde{\omega}_p^2}{\omega^2+\Gamma^2}\right] - i\varepsilon_r\left[\frac{\Gamma}{\omega}\frac{\widetilde{\omega}_p^2}{\omega^2+\Gamma^2}\right] \quad (6)$$

where

$$\widetilde{\omega}_p^2 = \frac{Ne^2}{m^*\varepsilon_0\varepsilon_r} \text{ and } \Gamma = \frac{e}{\mu m^*}.$$

In (6), the low-frequency dielectric constant ε_r is used to represent the response other than from the free carriers. This is a good approximation when the barrier's phonons have resonant frequencies higher than the Josephson frequency and the relevant harmonics. However, it is not clear whether this is a good approximation for the barrier materials of current interest.

Equation (6) is used to calculate the normal-state barrier conductance. Notice that for $\omega \neq 0$

$$G(\omega) = i\omega\varepsilon_0\varepsilon_r\frac{A}{d} = i\omega\varepsilon_0\varepsilon_r\left(\left[1 - \frac{\widetilde{\omega}_p^2}{\omega^2+\Gamma^2}\right] - i\left[\frac{\Gamma}{\omega}\frac{\widetilde{\omega}_p^2}{\omega^2+\Gamma^2}\right]\right)\frac{A}{d}$$
$$G_r(\omega) = \varepsilon_0\varepsilon_r\left[\Gamma\frac{\widetilde{\omega}_p^2}{\omega^2+\Gamma^2}\right]\frac{A}{d}$$
$$G_i(\omega) = \omega\varepsilon_0\varepsilon_r\left[1 - \frac{\widetilde{\omega}_p^2}{\omega^2+\Gamma^2}\right]\frac{A}{d}. \quad (7)$$

For $\omega = 0$

$$G(0) = i\omega\varepsilon_0\varepsilon(\omega)\left.\frac{A}{d}\right|_{\omega=0} = i\omega\varepsilon_0\varepsilon_r\left(\left[1 - \frac{\widetilde{\omega}_p^2}{\omega^2+\Gamma^2}\right] - i\left[\frac{\Gamma}{\omega}\frac{\widetilde{\omega}_p^2}{\omega^2+\Gamma^2}\right]\right)\frac{A}{d}$$
$$= \frac{\widetilde{\omega}_p^2}{\Gamma}\varepsilon_0\varepsilon_r\frac{A}{d} = \frac{1}{R_0}$$

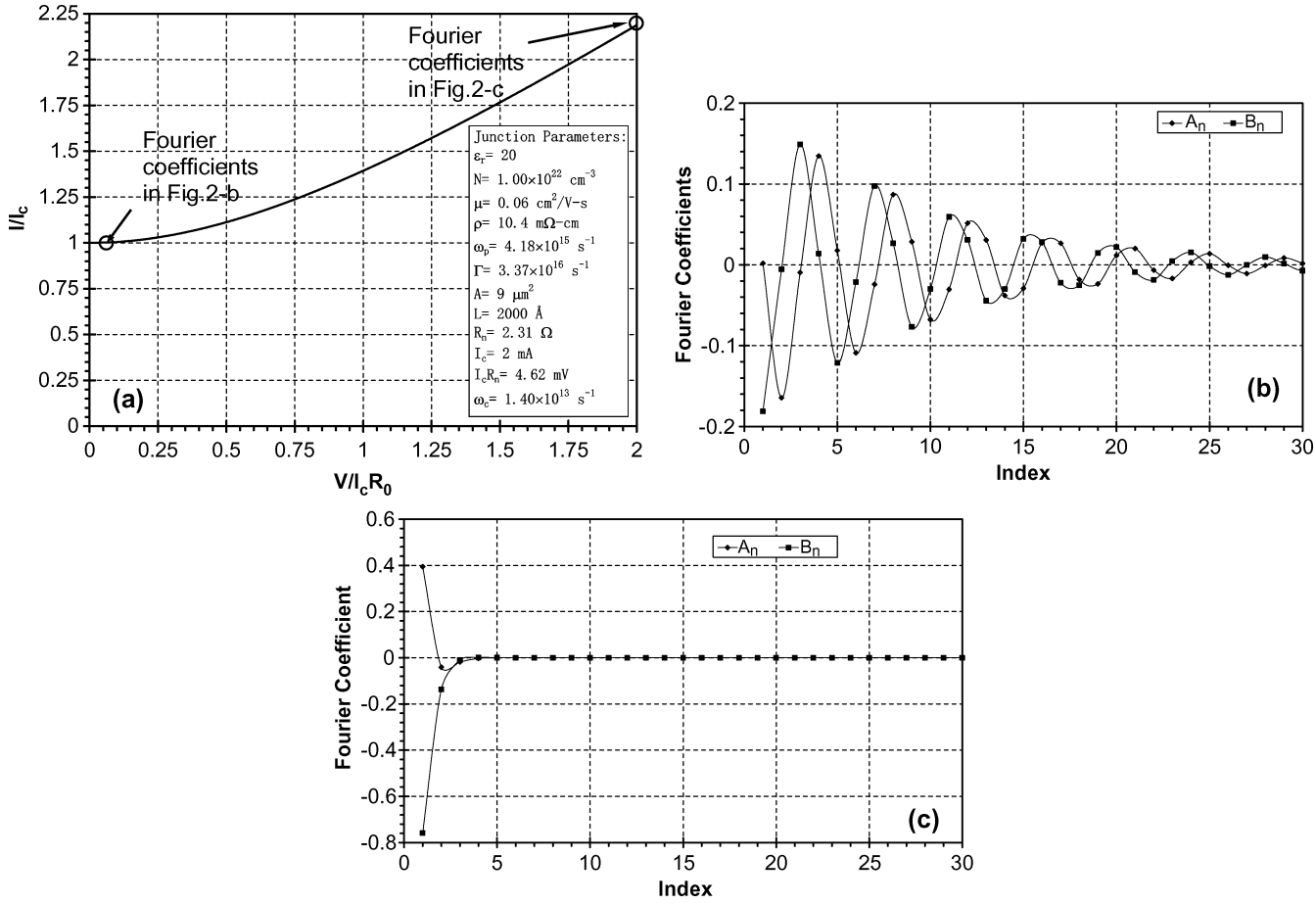

Fig. 2. (a) Representative calculation of an *I–V* characteristic of an SNS junction with a 200-nm 18 m$\Omega \cdot$cm barrier and a critical current of 2 mA. Corresponding Fourier coefficients, A_N and B_N, for bias current (b) $I = 1.0005 I_c$ and (c) $I = 2.118 I_c$, which corresponds to an average voltage of $0.1 I_c R_n$ and $2 I_c R_n$, respectively.

where R_0 is equal to the dc resistance of the normal barrier layer.

Furthermore

$$g_n = G_r(n\kappa\omega_C)R_0 = \frac{\Gamma^2}{\Gamma^2 + (n\kappa\omega_C)^2}$$

and

$$h_n = G_i(n\kappa\omega_C)R_0 = \left[\frac{\Gamma}{\widetilde{\omega}_p^2} - \frac{\Gamma}{\Gamma^2 + (n\kappa\omega_C)^2}\right] n\kappa\omega_C = \left[\frac{\Gamma^2}{\widetilde{\omega}_p^2} - g_n\right] \frac{\omega_C}{\Gamma} n\kappa\omega_C. \quad (8)$$

These values' results can now be directly used in (4) to obtain *I–V* characteristics using the method outlined in Appendix 2. To calculate *I–V* characteristics near $\langle V \rangle = 0$, the number of terms in the Fourier expansion quickly exceeds the computing capacity. Thus, we will not calculate *I–V* near $\langle V \rangle = 0$ for the discussion in this paper. We calculate the *I–V* curve when $\langle V \rangle$ is lowered from high voltages toward zero.

Until now, we have assumed a homogeneous barrier. In practice, there are other factors resulting from spatially nonuniform properties that may need to be included to accurately simulate practical junctions. For example, an interface boundary resistance caused by interfacial carrier or phonon scattering might be present. Also, semiconductor barriers might contain a region depleted of carriers and a nonuniform potential as a result of the formation of a Schottky barrier at the interfaces. Parasitic capacitances and inductances are often significant. These effects can be easily built into our generalized conductance model since series impedances and parallel conductances are additive. For example, the conductance of a barrier containing an interface boundary resistance $R_b(\omega)$ or a shunt parasitic capacitance $C_p(\omega)$ is $G(\omega) = G_{bulk}(\omega)/(G_{bulk}(\omega)R_b(\omega) + 1)$ and $G(\omega) = G_{bulk}(\omega) + i\omega C_p$, respectively. In many cases, for determining the critical current, an important input parameter to our model, complex and/or inhomogeneous geometries may need to be performed experimentally since it may be difficult to address theoretically with existing means. In either case, this is beyond the scope of this paper.

In the following section of this paper, we first give one representative set of results that includes both the calculated *I–V* characteristics and the Fourier coefficients of the junction voltage. To demonstrate the validity of our calculation scheme, we take the appropriate limit of (6) that is expected to generate results identical to that of McCumber's simpler RSJ model. After that, we report new theoretical results using the methodology that we developed for two barrier materials with conductivities near the metal–insulator transition: a conventional semiconductor with a relatively high mobility and a strongly scattered defect solid.

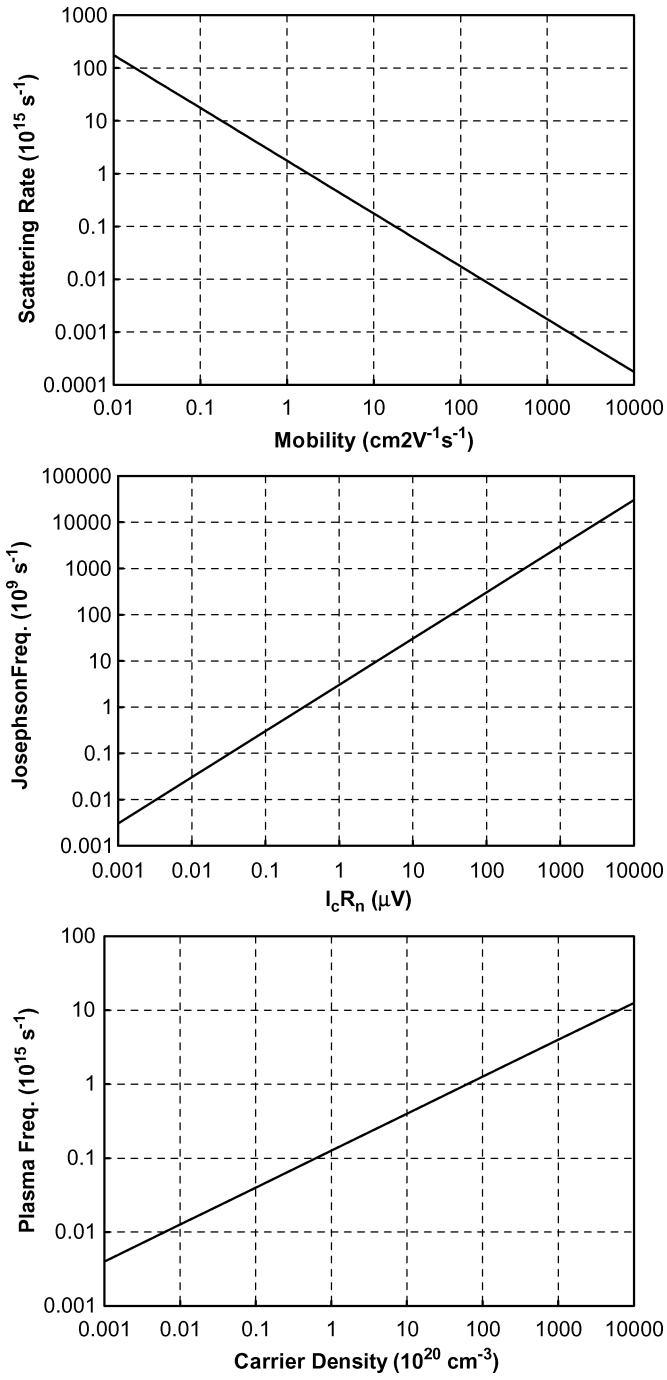

Fig. 3. (a) Scattering rate as a function of mobility, (b) Josephson frequency as a function of the I_cR_n product, and (c) plasma frequency as a function of carrier density. To calculate the plasma frequency, a carrier mass equal to the free electron mass and a dielectric constant of 20 was used. Plasma frequency of any material of interest can be determined by scaling the results in (c) by $\sqrt{(m_0/m^*)(20/\varepsilon_r)}$.

III. Results and Discussion

Fig. 2(a) shows an example of a calculated SNS junction *I–V* characteristic for a representative junction with a barrier resistivity near the metal–insulator transition. Fig. 2(b) illustrates the Fourier coefficients of the junction voltage. At large dc voltages corresponding to when κ is large (typically $\kappa > 2$ and $\langle V\rangle > 2I_cR_n$), the voltage oscillation is sine-like and very few

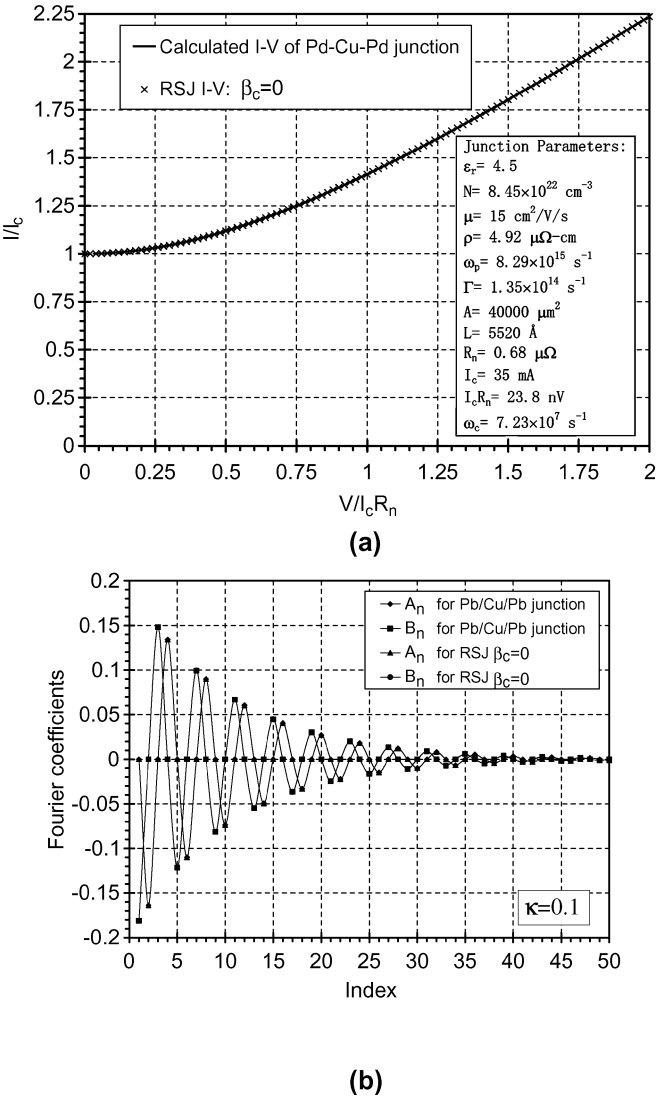

Fig. 4. (a) Calculated *I–V* characteristic and (b) Fourier coefficients of junction voltage at $\kappa = 0.1$ for Pb–Cu–Pb junction explored experimentally.

terms in the Fourier expansion significantly contribute to the response. As the dc voltage, and thus κ, is reduced in equal steps, more and more terms are needed, and the reduction in the total current becomes progressively smaller for each κ step.

1) Strong Scattering in the Barrier: To verify our calculation scheme, we set $g_n = 1$ and $h_n = n\kappa\beta_C$ in order to obtain the conductance $G(\omega) = (1/R_0)+i\omega C$ of the RSJ model. Thus, the RSJ model is mathematically equivalent to our model for this special case. The resulting *I–V* characteristics are illustrated in Fig. 1, and they are expected to be the solution to the RSJ model with an accuracy of no worse than $10^{-6}\%$. In the original work, McCumber calculated the *I–V* curves for a circuit with a frequency-independent parameter for the quasi-particle current using a numerical integration method that differs from our iterative Fourier expansion scheme. The curves directly taken from McCumber's work [1] are compared with our calculation results in Fig. 1. The agreement is excellent. Only at small normalized voltages do we find a small difference, which is most likely attributed to integration errors in the earlier work as a result of the limited computing power available at that time. Since the exact

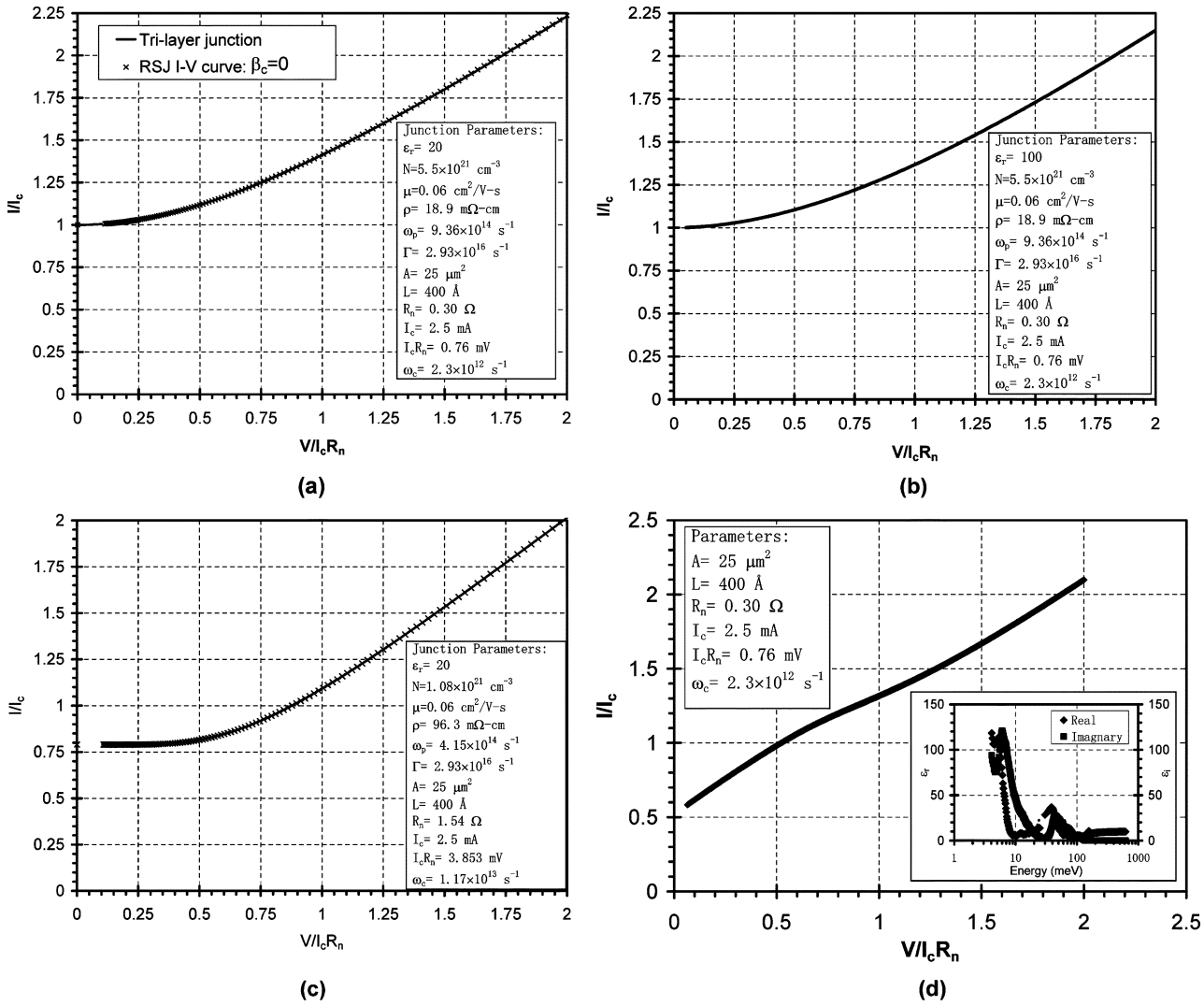

Fig. 5. (a) *I–V* characteristics with parameters chosen to simulate a prototypical strongly scattered defect barrier junction, such as our NbN–Ta_xN–NbN junctions. Solid line is calculated from our model. Since in this case $\Gamma \gg \omega_C$ and $\Gamma \gg \omega_p$, the RSJ model is expected to be a good approximation, and we find this to be a valid conclusion when we compare our results (solid line) and the RSJ model with $\beta_C = 0.077$ (crosses, ×). (b) Simulated NbN–Ta_xN–NbN junction with the same parameter used for Fig. 5(a) except increased ε_r to 100. No noticeable change in *I–V*. (c) Simulated Ta_xN junction that shows hysteretic behavior. In this figure, we compare our results (solid line) and the RSJ model with $\beta_C = 2.0$ (crosses, ×) and find good agreement as well. (d) Simulated *I–V* characteristics of NbN–Ta_xN–NbN junctions with measured dielectric function of Ta_xN (shown in the insert of the plot).

details of the calculation and corresponding accuracy are not documented in McCumber's paper [1], it is not possible for us to make a more accurate comparison. However, the comparison presented above does show that our iterative scheme and McCumber's integration scheme both yielded essentially the same solution.

In general, the RSJ model is valid when the time between quasi-particle scattering events in the barrier $(1/\Gamma)$ is significantly shorter than both the period of voltage oscillation across the junction $(1/\omega_C)$ and the period of the barrier material's plasma frequency $(1/\omega_p)$. In this case, the electrodynamic response of the quasi-particles in the barrier is resistive in nature and

$$G(\omega) = i\omega\varepsilon_0\varepsilon_r\left(\left[1-\frac{\widetilde{\omega}_p^2}{\omega^2+\Gamma^2}\right]-i\left[\frac{\Gamma}{\omega}\frac{\widetilde{\omega}_p^2}{\omega^2+\Gamma^2}\right]\right)\frac{A}{d}$$
$$\approx \frac{\widetilde{\omega}_p^2}{\Gamma}\varepsilon_0\varepsilon_r\frac{A}{d}+i\omega\varepsilon_0\varepsilon_r\frac{A}{d} = G(0)+i\omega C = \frac{1}{R_0}+i\omega C$$

where $C = \varepsilon_0\varepsilon_r(A/d)$, $R_0 = \Gamma/\tilde{\omega}_p^2 C = 1/G(0)$. Thus, the quasi-particle current is in-phase with the voltage, the impedance of the junction is dissipative and equal to $R_0 = \rho_0 A/d$, and the junction can therefore accurately be simulated by the RSJ model with $\beta_C = (2e/\hbar)CI_cR^2 = \Gamma\omega_C/\tilde{\omega}_p^2$.

If we consider the case with more carriers in the barrier, the magnitude of Γ can become on the same order or smaller than $\widetilde{\omega}_p$. With strong scattering $\Gamma \gg \omega_C$, and (8) predicts that in this limit g_n and h_n are

$$g_n = 1, \quad \text{and} \quad h_n = \beta_{\text{eff}} n\kappa$$

where $\beta_{\text{eff}} = \omega_C[\Gamma/\widetilde{\omega}_p^2 - 1/\Gamma] = h_n/n\kappa$. To distinguish β_{eff} from β_C in the RSJ circuit model, which is defined in terms of circuit elements, we introduce β_{eff}, which is defined from barrier material properties. Similar to the role of β_C, β_{eff} determines the extent of hysteresis in the strong scattering limit. In this case, the relationship between β_{eff} and $(I/I_c)_{\min}$ is given by Fig. 1(b) with β_{eff} instead of β_C on the vertical axis.

To assist the reader in comparing the different limits, we have plotted in Fig. 3 the scattering rate as a function of mobility, the Josephson frequency as a function of the I_cR_N product, and the plasma frequency as a function of carrier density. To calculate the plasma frequency, we assume that the carrier mass and the static dielectric constant, ε_r, are equal to the free electron mass and 20, respectively. These results can be scaled by $\sqrt{(m_0/m^*)(20/\varepsilon_r)}$ to determine the plasma frequency for any material of interest.

We next model junctions with conventional metal barriers. Fig. 4 illustrates the simulation of Pb–Cu–Pb junctions which have been explored experimentally in [6]. In this case, $\Gamma \gg \omega_C$ and $\Gamma < \widetilde{\omega}_p$. This results in all of the g_n being very close to 1 and the $\beta_{\text{eff}} \approx [(\Gamma^2/\widetilde{\omega}_p^2) - 1]\omega_C/\Gamma$ being small and negative as a result of $0 > [(\Gamma^2/\widetilde{\omega}_p^2) - 1] > -1$ and $(\omega_C/\Gamma) \ll 1$. The RSJ model predicts β_C is essentially equal to 0. Our model predicts essentially identical *I–V* characteristics and Fourier coefficients for the junction voltages to those predicted by the RSJ model, as indicated in Fig. 4.

Our last simulation of a junction with a barrier in the strongly scattered limit uses device parameters (i.e., dimensions, I_c, and R_n) from optimized nonhysteretic junctions with a Ta_xN barrier tuned near the metal–insulator transition, as reported in [5] and [11]. For simplicity, we use a constant dielectric constant ε_r of 20 as this value is obtained for optical measurements in the visible range. This approximation will be examined in the next paragraph. For this system, the carriers are very strongly scattered in the barrier [12] and $\Gamma \gg \omega_C$ and $\Gamma \gg \omega_p$. Therefore, the RSJ model is expected to be consistent with our model. One junction described by [5] has I_c of 2.5 mA, R_n of 0.3 Ω, and I_cR_n of 0.75 mV. Using these junction parameters, we calculated a $\beta_C = (2e/\hbar)CI_cR^2 \approx 0.077$ for the RSJ model. Furthermore, we found g_n close to 1 and $\Gamma\omega_C/\widetilde{\omega}_p^2$ close to $\beta_{\text{eff}} = 0.077$ for our model, consistent with the analysis for the limiting case discussed in the previous section. Fig. 5(a) shows that the calculation based on our model appears to be identical with the RSJ model of $\beta_C = 0.077$. Note that there are significant discrepancies between the experiment and the predictions of the two models. This cannot be reconciled by using a dielectric constant as high as 100 [Fig. 5(b)]. This will be discussed further in the next paragraph. We also show that the shape of the *I–V* curve is relatively insensitive to compensating changes in carrier concentration and mobility when the resistivity and other parameters are fixed, as illustrated in Fig. 6. For this junction system, we have also modeled other *I–V* characteristics with more hysteresis [Fig. 5(c)] [11] and find that the result is consistent with the RSJ model of $\beta_C \approx 2$. The agreement between our model and the RSJ model in these cases showed that the dynamic response of the free carriers has almost no effect on the *I–V* characteristics in the strongly scattered limit.

In [5] and [11], the measured *I–V* curves in Ta_xN junctions show "excess current," extrapolation of the high-voltage part of the *I–V* characteristic to the zero-voltage axis intersects at a positive current. This type of behavior is predicted by neither the RSJ model nor our calculations based on a frequency-independent dielectric constant [e.g., Fig. 5(a) and (c)]. We have inferred the frequency-dependent dielectric constant of Ta_xN films from

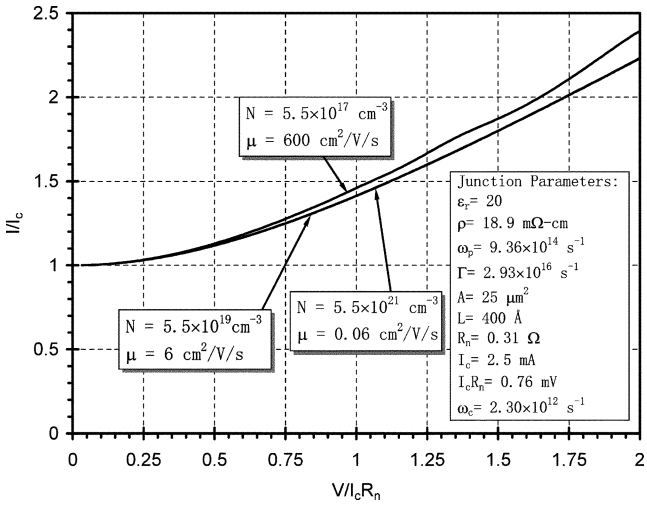

Fig. 6. Calculated *I–V* characteristics with parameters similar to those in Fig. 5, except the mobility is increased and carrier density decreased while keeping all other parameters including resistivity, device dimensions, and the critical current unchanged. First few orders of magnitude change in mobility and carrier density have almost no effect on the shape of the *I–V* curve. *I–V* curve is essentially the $\beta_C = 0.077$ curve for the RSJ model (see Fig. 5). However, in the case of very high mobility, the RSJ model is not expected to be valid and our model's calculation of the *I–V* characteristics predicts currents significantly above the RSJ $\beta_C = 0.077$ curve.

preliminary optical measurements[1] [insert in Fig. 5(d)]. The use of this dielectric function along with other parameters for Ta_xN in our model results in an *I–V* curve [Fig. 5(d)] which shows excess current and is similar in shape to the *I–V* characteristics illustrated in [5] and [11]. The excess current-like feature in the *I–V* is a direct consequence of the drastic change in dielectric function near 3 meV. There still are differences between the later calculation and experiment data, such as the amount of hysterisis. Nevertheless, this example shows that various dispersion and dissipation mechanisms can be incorporated in our models of the *I–V* characteristics. Thus, our model can provide insight to the operation of a variety of Josephson junctions.

2) Weak Scattering in the Barrier: For many barrier materials with relatively high mobility, the criterion that Γ is much larger than both $\widetilde{\omega}_p$ and ω_C is not satisfied. For such cases, the dependence of h_n on n becomes more complicated and we expect the shape of the *I–V* characteristics to deviate from those that can be predicted by the RSJ model. This result is because the conductance of the barrier material also contains an out-of-phase component, which is a result of the inertia of the carriers causing a time lag in their response in a time-varying field and is most significant for materials with reduced carrier scattering and, thus, higher mobility. The free carriers' dynamic response is typically modeled with a resistor representing the in-phase scattering loss and an inductor for the out-of-phase dispersive response. The inductive term results from the inertia

[1]The conductivity of Ta_xN films can be varied over a wide range by adjusting the stoichiometry. To measure the dielectric response of the Ta_xN lattice, the properties of a nonconductive Ta_xN film was measured. A Brucker Model IFS 86 W/S spectrometer was used in the range of photon energies between 3.5 and 25 meV and a Woolam Co ellipsometer Model IR-VASE was used for photon energies between 30 and 650 meV. The dc dielectric constant was determined from a 1-MHz capacitance measurement of a Nb–Ta_xN–Nb parallel plate structure. These results in combination with the model of the free carrier dielectric constant (6) were used to infer the dielectric response of the Ta_xN.

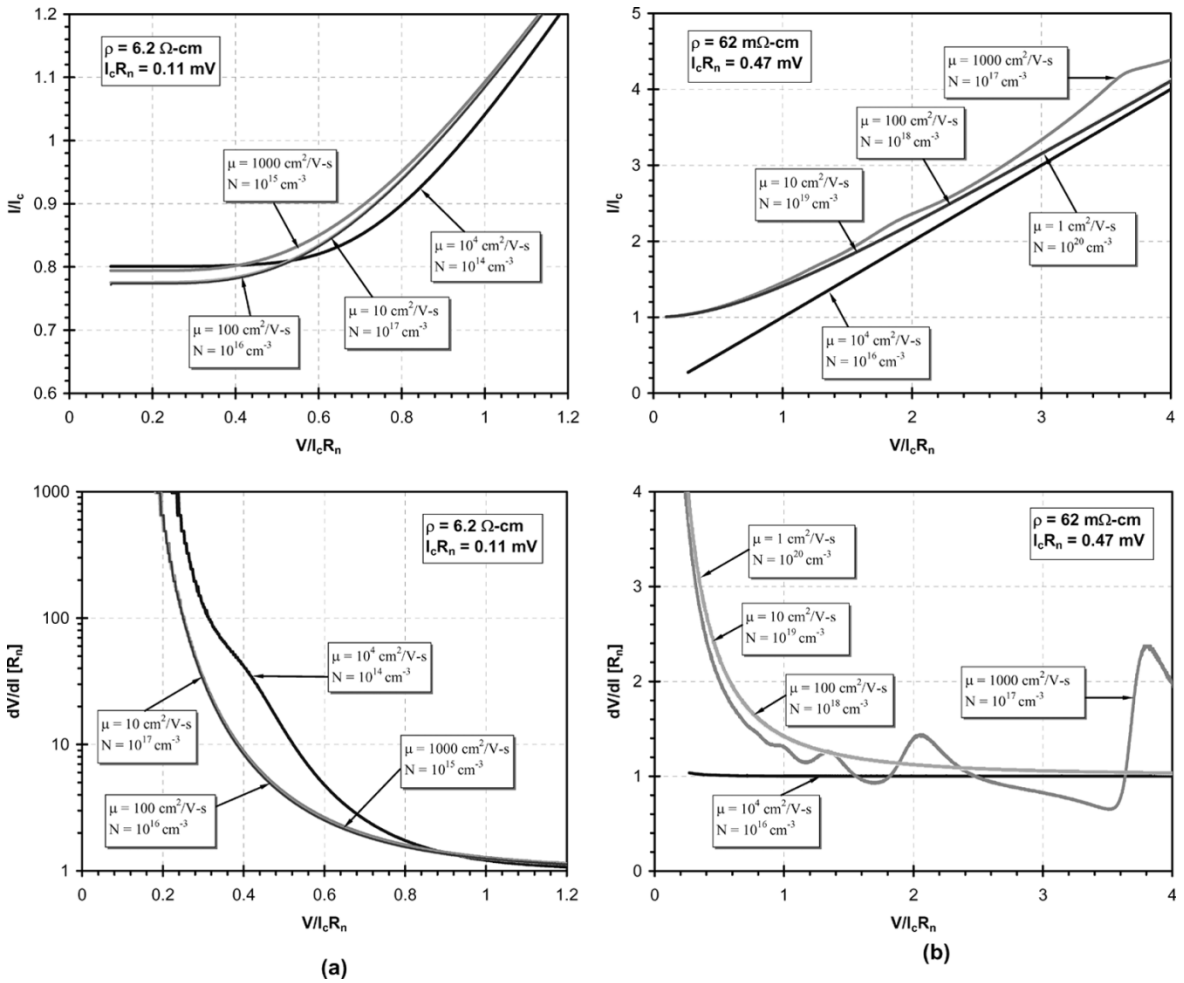

Fig. 7. Calculation of *I–V* characteristics of a junction comprising Nb electrodes and a relatively high-mobility barrier with resistivities of $\sim$ 60 m$\Omega \cdot$ cm and 6 $\Omega \cdot$ cm. Barrier's dielectric parameters are those of Si and are listed in Tables I and II: (a) $\rho = 6.2\ \Omega \cdot$ cm, $I_cR_n = 0.13$ mV and (b) $\rho = 62$ m$\Omega \cdot$ cm, $I_cR_n = 0.56$ mV.

of the free carriers. For this high mobility case, the average carrier is not scattered in a period of oscillation of the field, and therefore the charge density and resulting polarization lags the electric field by 90°. This results in the electrical circuit equivalent of an inductive response, even though the resulting stored energy arises from an electric field. We will show that the free carriers' dynamic response causes the electrical properties of these junctions to differ from the predictions of the RSJ model.

To illustrate the influence of this effect we simulate a set of Nb–Si–Nb junctions with various carrier densities and mobilities for the barrier. Si was selected to be the barrier material since it is the most common semiconductor, can be formed with a very large range of mobility and carrier density, and can be easily tuned through the metal–insulator transition. In practice, depending on the method of preparation, a Schottky barrier can form at the Nb–Si interfaces [13]. To simplify our analysis, we shall ignore the potential Schottky barrier, assuming ohmic contacts. This situation can be realized in practice by using delta-doped layer at the Nb–Si interface. We are going to compare the junctions having the same ρ_0 and I_cR_n product, since such junctions have the same McCumber number $\beta_C = (2e/\hbar)I_cR_n(\varepsilon_0\varepsilon_r(A/d))(\rho_0(d/A)) = (2e/\hbar)I_cR_nCR_n$, hence identical *I–V* characteristics are predicted by the RSJ model. Thus, the differences that are observed can be attributed to the dynamic response of free carriers in the barrier.

We next compare the predictions of our model with the RSJ model for junctions with barriers that have a wide range of mobilities. In order to illustrate the difference, we adjust the barrier properties so that the two key parameters of the RSJ model, I_c and β_C, are kept constant. For these cases, the RSJ model predicts identical *I–V* curves and we again show that our model differs significantly for the high mobility case.

In order to perform the calculations, we first need to select relevant values for the critical current, an input parameter in both our model and the RSJ model. We choose the simplest available formulation to illustrate this point. For junctions in the dirty limit ($l_p \ll \xi_{nd}$), we use Likharev's analytical SNS model [4], [9], [18], [19] to predict the I_c

$$I_cR_n = \frac{4}{\pi e}\frac{|\Delta|^2}{k_BT_C}\frac{d}{\xi_{nd}}\exp\left(-\frac{d}{\xi_{nd}}\right),\ \text{valid for } 0.3T_C < T < T_C$$

where $\xi_{nd} = \sqrt{\hbar D/2\pi k_BT_C}$ is the normal metal coherence in the dirty limit, and D[2] is the diffusivity. Within Likharev's model, I_cR_n is fixed when d/ξ_{nd}, the ratio between barrier

[2]For materials with a thermal velocity larger than Fermi velocity (i.e., $N < 10^{18}/\text{cm}^3$), the nondegenerate Einstein relationship expression $D = (k_BT/e)\mu$ is used to infer the diffusivity. For higher carrier concentrations, the degenerate expression $D = (1/3)v_Fl$ is used.

TABLE I
JUNCTION PARAMETERS USED FOR FIG.7(a)

Junction Parameter	Symbol					Units
Dielectric constant	ε_r	11.9	11.9	11.9	11.9	
Critical temperature	T_C	9.2	9.2	9.2	9.2	K
Temperature	T	4.2	4.2	4.2	4.2	K
Energy gap x2	2Δ	2.8	2.8	2.8	2.8	meV
Carrier density	N	1.0×10^{17}	1.0×10^{16}	1.0×10^{15}	1.0×10^{14}	cm^{-3}
Fermi velocity	v_f	1.9×10^{4}	1.5×10^{4}	1.5×10^{4}	1.5×10^{4}	m/s
Thermal velocity	v_{th}	1.5×10^{4}	1.5×10^{4}	1.5×10^{4}	1.5×10^{4}	m/s
Mobility	μ	10	100	1000	10000	$cm^2/V/s$
Resistivity	ρ	6.2×10^{3}	6.2×10^{3}	6.2×10^{3}	6.2×10^{3}	$m\Omega$-cm
Plasma frequency	ω_p	5.5×10^{12}	1.8×10^{12}	5.5×10^{11}	1.8×10^{11}	s^{-1}
Scattering rate	Γ	2.0×10^{14}	2.0×10^{13}	2.0×10^{12}	2.0×10^{11}	s^{-1}
Mean free path	l_p	0.1	0.7	7.3	73.3	nm
N-M coherence length	ξ_{nd}	0.42	1.0	3.2	10.2	nm
N-M coherence length	ξ_{nc}	5.5	4.3	4.3	4.3	nm
N-M coherence length	ξ_n	0.42	1.0	3.2	4.3	nm
Junction area	A	9.0	9.0	9.0	9.0	μm^2
Thickness	L	2.1	5.1	16.2	16.2	nm
Residual resistance	R_n	14.5	35.5	112.2	112.3	Ω
Critical current	I_c	0.0073	0.0030	0.00095	0.00095	mA
I_cR_n	I_cR_n	0.11	0.11	0.11	0.11	mV
Josephson frequency	ω_C	3.2×10^{11}	3.2×10^{11}	3.2×10^{11}	3.2×10^{11}	s^{-1}
Limit used		dirty	dirty	dirty	clean	

thickness and ξ_{nd}, is constant. For junctions in the clean limit ($l_p \gg \xi_{nc}$), the junction I_c is predicted to vary as

$$I_c = I_{C0}\exp\left(-\frac{d}{\xi_{nc}}\right)$$

where $\xi_{nc} = (\hbar/2\pi k_B T)v_F$ [14] for degenerate semiconductor barriers and $\xi_{nc} = (\hbar/2\pi k_B T)v_{th} = \hbar\sqrt{3/4\pi^2 k_B T m^*}$ for nondegenerate semiconductors. In the latter case, ξ_{nc} does not directly depend on mobility or carrier concentration.

The modeling of junctions with dc barrier resistivities of ~ 62 m$\Omega\cdot$cm and 6.2 $\Omega\cdot$cm is presented in Fig. 7. To obtain the curves in Fig. 7, we began by selecting a resistivity ρ_0 and a mobility in the dirty limit and a barrier thickness d that is several times the ξ_{nd} so that Likharev's analytical SNS model is valid. We then increase the barrier mobility and decrease the carrier concentration while keeping d/ξ_{nd} constant. At a sufficiently high mobility, when the material is in the clean limit, we vary d/ξ_{nc} to continue to maintain the same I_cR_n. In the highest mobility cases, the mean-free path becomes longer than the barrier thickness and significant levels of ballistic quasi-particle current can flow through the barrier. In practice, such a junction has been realized using high-mobility semiconductor barriers, such as InAs [16].

As can be seen in Fig. 7, the result for junctions with high mobility barriers differ both qualitatively and quantitatively from the predictions of the RSJ model. Fig. 7 shows that there can be "bumps" at several nonzero voltages. For the purpose of our discussion, we refer to these voltages as critical regions. These features are associated with the occurrence of the barrier's plasma frequency near the characteristic frequency of the junction. For the range of barrier resistivities being investigated here (i.e., near the metal–insulator transition), this occurs only in the high-mobility materials. Several critical regions are illustrated in detail in Fig. 8. If h_n is large in the critical region, the anomaly can be hysteretic [Fig. 8(a)].

Quantitative analysis indicates that the critical regions occur when one of the h_n is zero, i.e.,

$$h_n = \left[\frac{\Gamma}{\widetilde{\omega}_p^2} - \frac{\Gamma}{\Gamma^2 + (n\kappa\omega_C)^2}\right] n\kappa\omega_C = 0$$
$$\Rightarrow \widetilde{\omega}_p^2 = \Gamma^2 + (n\kappa\omega_C)^2 \Rightarrow \kappa = \frac{1}{n\omega_C}\sqrt{\widetilde{\omega}_p^2 - \Gamma^2}.$$

This condition occurs when the plasma frequency and scattering rate couple in such a way that the real part of the dielectric constant of the system is zero for a specific frequency component of the response (i.e., a given index, n). This follows since h_n, G_i, and the real part of the dielectric constant, i.e., the first term in (6), are all zero. The applied voltage V, at which this occurs, is equal to $\hbar/2en\sqrt{\widetilde{\omega}_p^2 - \Gamma^2}$, where $\widetilde{\omega}_p$ is the barrier's plasma frequency, n is an integer, Γ is the scattering rate, and $\hbar$ is the reduced Planck constant.

Studies in the literature report semiconductor and semimetal barrier junction *I–V* characteristics with anomalies below the energy gap that resemble these critical regions and whose physical mechanism has not previously been identified. For

TABLE I
JUNCTION PARAMETERS USED FOR FIG. 7(b)

Junction Parameter	Symbol						Units
Dielectric constant	ε_r	11.9	11.9	11.9	11.9	11.9	
Critical temperature	T_C	9.2	9.2	9.2	9.2	9.2	K
Temperature	T	4.2	4.2	4.2	4.2	4.2	K
Energy gap x2	2Δ	2.8	2.8	2.8	2.8	2.8	meV
Carrier density	N	1.0×10^{20}	1.0×10^{19}	1.0×10^{18}	1.0×10^{17}	1.0×10^{16}	cm^{-3}
Fermi velocity	v_f	1.9×10^{5}	8.9×10^{4}	4.1×10^{4}	1.9×10^{4}	1.5×10^{4}	m/s
Thermal velocity	v_{th}	1.5×10^{4}	1.5×10^{4}	1.5×10^{4}	1.5×10^{4}	1.5×10^{4}	m/s
Mobility	μ	1	10	100	1000	10000	$cm^2/V/s$
Resistivity	ρ	62.4	62.4	62.4	62.4	62.4	$m\Omega$-cm
Plasma frequency	ω_p	1.8×10^{14}	5.5×10^{13}	1.8×10^{13}	5.5×10^{12}	1.8×10^{12}	s^{-1}
Scattering rate	Γ	2.0×10^{15}	2.0×10^{14}	2.0×10^{13}	2.0×10^{12}	2.0×10^{11}	s^{-1}
Mean free path	l_p	0.095	0.44	2.0	9.5	73.3	nm
N-M coherence length	ξ_{nd}	1.3	1.9	2.8	4.2	10.2	nm
N-M coherence length	ξ_{nc}	55.3	25.7	11.9	5.5	4.3	nm
N-M coherence length	ξ_n	1.3	1.9	2.8	4.2	4.3	nm
Junction area	A	9.0	9.0	9.0	9.0	9.0	μm^2
Thickness	L	4.0	5.8	8.5	12.5	7.5	nm
Residual resistance	R_n	0.27	0.40	0.59	0.87	0.52	Ω
Critical current	I_c	1.7	1.2	0.79	0.54	2.8	mA
I_cR_n	I_cR_n	0.47	0.47	0.47	0.47	0.47	mV
Josephson frequency	ω_C	1.4×10^{12}	1.4×10^{12}	1.4×10^{12}	1.4×10^{12}	1.4×10^{12}	s^{-1}
Limit used		dirty	dirty	dirty	dirty	clean	

example, Fig. 9 shows possible evidence for critical regions in the *I–V* curve of Si single-crystal membrane barrier junction near 0.42 and 0.21 mV reported by Huang and Van Duzer [6]. Other studies have also observed similar features, as in the case of [16, Fig. 3(b)]. In that study, the measured R_N indicates that the barrier is partially depleted, therefore we are not able to confidently estimate the carrier concentration within the barrier and therefore cannot unequivocally attribute this anomaly to the barrier's plasma frequency.

The critical features may be distinguished from other subgap features by their energy and temperature dependences. The subharmonic gap feature associated with the electrode's gap falls at voltages equal to $2\Delta/m$ (where m is an integer) and will have the characteristic temperature dependence of the energy gap [16], [17]. In contrast, the critical region's voltage depends on $\widetilde{\omega}_p$, Γ, and I_cR_n. If the barrier falls on the insulator side of the MI transition, $\widetilde{\omega}_p$ will drop dramatically as carrier freeze-out occurs at low temperature. If the barrier falls on the metallic side, the critical region's voltage would not generally coincide with the gap features and the temperature dependence would be relatively constant since Γ and $\widetilde{\omega}_p$ are both expected to have weak temperature dependence. The former will typically be dominated by impurity scattering $(T^{3/2})$, and the latter depends primarily on the carrier density.

The dielectric function model given by (6) is a special case of the Lorentz oscillator model for the dielectric function [10] with a single oscillator centered at zero frequency. There are many other processes in solids, for examples excitation from defects or phonons, that are modeled with oscillators at nonzero frequencies. Consider the simplest case where a single oscillator is centered at $\omega_0 > 0$. The dielectric function takes on the following form:

$$\varepsilon(\omega) = \varepsilon_r \left[1 - \frac{\widetilde{\omega}_p^2\left(\omega_0^2 - \omega^2\right)}{\left(\omega_0^2 - \omega^2\right)^2 + \Gamma^2\omega^2}\right] - i\varepsilon_r \left[\frac{\widetilde{\omega}_p^2\Gamma\omega}{\left(\omega_0^2 - \omega^2\right)^2 + \Gamma^2\omega^2}\right]$$

where Γ is the oscillator width and $\widetilde{\omega}_p$ corresponds to the oscillator strength. In this case

$$g_n = n\kappa\omega_C C_0\varepsilon_r R_0 \frac{\widetilde{\omega}_p^2\Gamma n\kappa\omega_C}{\left(\omega_0^2 - (n\kappa\omega_C)^2\right)^2 + \Gamma^2(n\kappa\omega_C)^2}$$

$$h_n = n\kappa\omega_C C_0\varepsilon_r R_0 \left[1 + \frac{\widetilde{\omega}_p^2\left(\omega_0^2 - (n\kappa\omega_C)^2\right)}{\left(\omega_0^2 - (n\kappa\omega_C)^2\right)^2 + \Gamma^2(n\kappa\omega_C)^2}\right].$$

Thus, we expect the critical region to occur at $h_n = 0$

$$\kappa = \frac{1}{n\omega_C}\sqrt{\omega_0^2 + \frac{\left(\widetilde{\omega}_p^2 - \Gamma^2\right) \pm \sqrt{\left(\widetilde{\omega}_p^2 - \Gamma^2\right)^2 - 4\Gamma^2\omega_0^2}}{2}}$$

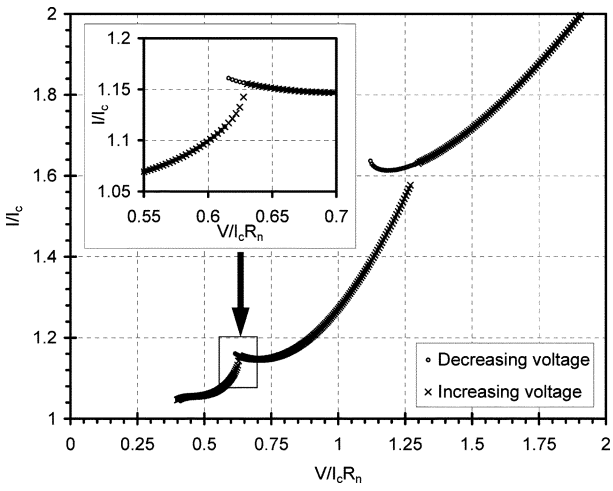

(a)

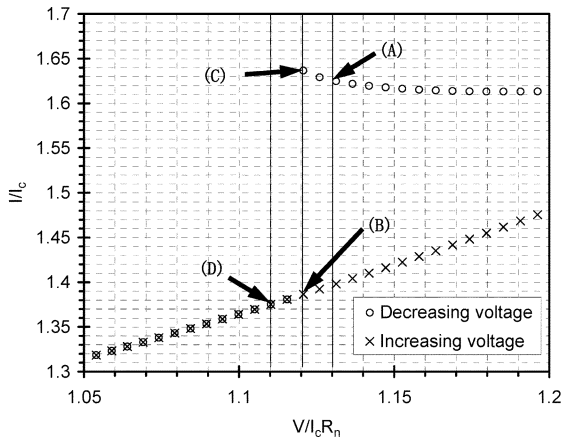

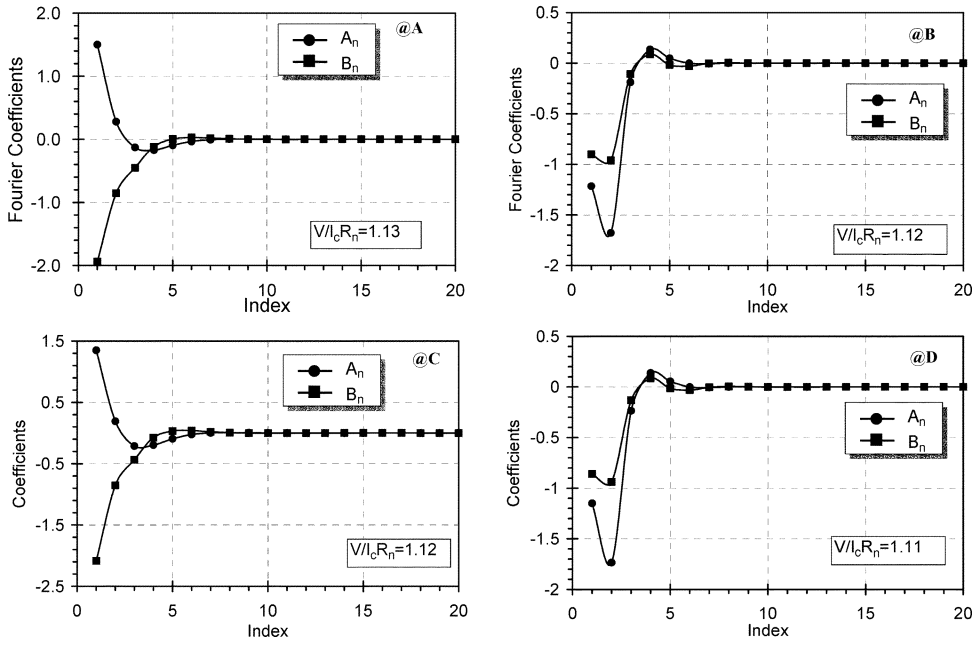

(b)

Fig. 8. In some cases, *I–V* curves with critical regions are observed, as shown here. (a) Hysteretic behavior can be seen in each of these regions. (b) *I–V* characteristics and Fourier coefficients at voltages focus in on the upper critical region of (a). Parameters are listed in Table III.

TABLE III
JUNCTION PARAMETERS USED FOR FIG. and 8(a)

Junction Parameter	Symbol		Units
Dielectric constant	ε_r=	11.9	
T_c	T_c=	9.2	K
Temperature	T=	1.2	K
Energy gap x2	2Δ=	3	meV
Carrier density	N=	1.25×10^{17}	cm^{-3}
Fermi velocity	v_f=	18000	m/s
Mobility	μ=	800	$cm^2/V/s$
Resistivity	ρ=	62.4	$m\Omega$-cm
Plasma frequency	ω_p=	5.78×10^{12}	s^{-1}
Scattering rate	Γ=	2.20×10^{12}	s^{-1}
Mean free path	l_p=	81.5	Å
N-M coherence length	ξ_n=	19.6	Å
Junction area	A=	25	μm^2
Thickness	L=	19.6	Å
Residual Resistance	R_n=	0.049	Ω
Critical Current	I_c=	28.1	mA
I_cR_n	I_cR_n=	1.37	mV
Josephson Freq	ω_c=	4.18×10^{12}	s^{-1}

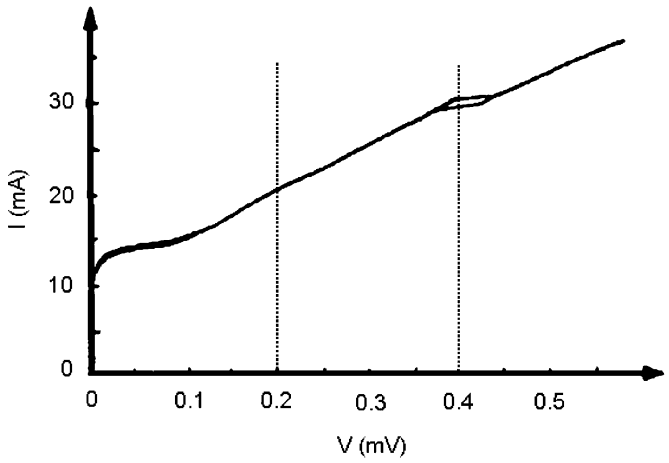

Fig. 9. *I–V* characteristic of a junction with a single-crystal Si membrane barrier. Regions that possibly could be associated with critical regions are observed at 0.42 and 0.21 mV.

when Γ is small and ω_0 is the dominant frequency. The expression can be simplified as

$$\kappa = \frac{\omega_0}{n\omega_C}.$$

Quasi-particle transport by tunneling and/or Andreev reflection is enhanced at a voltage corresponding to the superconducting energy gap 2Δ. This can be incorporated into the model using oscillators centered at $\omega_0 = 2\Delta$ in the dielectric function. In this case, our simulated *I–V* will yield subgap harmonic structures as in [16] and [17].

IV. CONCLUSION

We have extended the (RSJ) circuit model to incorporate a frequency-dependent dielectric response so that mechanisms of dissipation and dispersion in the barriers can be taken into account. Since the method we developed can solve the nonlinear junction equations for a barrier with an arbitrary complex conductivity, it is also capable of including other relevant processes within the barrier, including the influence of excitation from shallow defects or very soft phonon modes, as well as boundary resistances. We have shown that the incorporation of the response of free carriers in SNS junctions significantly influences the dc *I–V* characteristics for the case of material near the metal–insulator transition with high mobility. Hysteretic anomalies occur at nonzero voltages in the *I–V* characteristics associated with the barrier layer's plasma frequency. The resulting features, which we call critical regions, occur when the dc junction voltage $\langle V \rangle$ is equal to $(\hbar/2en)\sqrt{\widetilde{\omega}_p^2 - \Gamma^2}$, where $\widetilde{\omega}_p$ is the barrier's plasma frequency, Γ is the quasi-particle scattering rate, n is an integer, and $\hbar$ is the reduced Planck's constant. We also show that our results for SNS junctions with a low-mobility barrier material are essentially identical to the predictions of the simpler RSJ model.

APPENDIX I
PROOF OF THE RELATIONSHIP BETWEEN AVERAGE JUNCTION VOLTAGE AND FUNDAMENTAL FREQUENCY OF JUNCTION VOLTAGE OSCILLATION

In this appendix, we explicitly show that the constant A_0, which sets a lower bound for the average normalized current r, is equal to κ.

Using the definition of normalized voltage γ in (3), the time average $\langle\gamma\rangle$ can be expressed as

$$\langle\gamma\rangle = \left\langle \frac{d\phi}{d\theta} \right\rangle = \frac{\kappa}{2\pi} \int_{\theta=0}^{\frac{2\pi}{\kappa}} \frac{d\phi}{d\theta} d\theta = \frac{\kappa}{2\pi} \int_{\theta=0}^{\frac{2\pi}{\kappa}} d\phi. \qquad \text{(A1-1)}$$

For a Josephson junction, every period of voltage oscillation corresponds to a change of 2π in the gauge-invariant phase, that is

$$\int_{\theta=0}^{\frac{2\pi}{\kappa}} d\phi = 2\pi. \qquad \text{(A1-2)}$$

Combine (A1-1) and (A1-2), and γ can be further expressed as

$$\langle\gamma\rangle = \kappa. \qquad \text{(A1-3)}$$

The above equation is true as long as voltage oscillation is periodic, regardless of its shape.

Also, since $\gamma = A_0 + \sum_{n=1}^{\infty}[A_n \cos(n\kappa\theta) + B_n \sin(n\kappa\theta)]$, we have $\langle\gamma\rangle = A_0$. Thus, we obtained following expression between the normalized average voltage A_0 and normalized fundamental frequency κ

$$A_0 = \kappa. \qquad \text{(A1-4)}$$

APPENDIX II
ITERATIVE ALGORITHM FOR DETERMINING THE I–V CHARACTERISTIC

The following numerical algorithm is used to calculate the junction *I–V* characteristics.

Step 1) Set initial upper bound for κ.

Step 2) Set up the initial conditions. First, guess the Fourier expansion coefficients $A_n s$ and $B_n s$ for $d\phi/d\theta$. Since the voltage oscillations are sinusoidal at high values of κ, a sine wave (i.e., $A_1 = 1$ with the remain coefficients set to zeros) is used as the initial guess. This is an efficient method to achieve convergence. Then, calculate $g_n s$ and $h_n s$ for this particular value of κ using their definitions.

Step 3) Calculate the expansion for ϕ. According to (3), the expansion for ϕ is determined by ϕ_0 and previously guessed values of $A_n s$ and $B_n s$. Without losing generality, one can choose ϕ_0 to be zero.

Step 4) Calculate $r = \langle \sin(\phi) \rangle + \kappa$.

Step 5) Use numerical integration to find Fourier coefficients for $\sin(\phi)$

$$\frac{\kappa}{\pi} \int_0^{\frac{2\pi}{\kappa}} \sin(\phi) \cos(n\kappa\theta) d\theta = C_n$$

$$\frac{\kappa}{\pi} \int_0^{\frac{2\pi}{\kappa}} \sin(\phi) \sin(n\kappa\theta) d\theta = D_n.$$

According to (4)

$$C_n = -g_n A_n - h_n B_n$$
$$D_n = -g_n B_n + h_n A_n.$$

Then, solve to get new A_n and B_n from

$$A_n = \frac{h_n D_n - g_n C_n}{g_n^2 + h_n^2}$$
$$B_n = \frac{-h_n C_n - g_n D_n}{g_n^2 + h_n^2}.$$

Step 6) Perform a weighted average with the new calculated coefficients and the values from the last iteration.

Step 7) Check the convergence condition for r. If not satisfied, go to Step 2). If satisfied, record r and κ.

Step 8) Reduce value for κ, and go to Step 2). Iteration will continue until r is calculated for all the desired the values of κ.

The above outlined method is effective when calculating *I–V* as average voltage reduces; we can trivially extend the scheme to the case when average voltage increases. However, in practice, as the average voltage approaches zero, the junction voltage is sharply peaked, and the number of Fourier terms required increases quickly to exceed the limit of computation capacity. Thus, when investigating the hysteresis at zero voltage, only the "return" part of the *I–V* can be obtained from this calculation.

ACKNOWLEDGMENT

The authors would like to thank Dr. A. M. Kadin and Dr. A. W. Kleinsasser for enlightening discussions as well as Dr. T. Tiwald and the J. A. Woollam Co., Inc., for collaborative work on measuring the dielectric function of Ta_xN.

REFERENCES

[1] D. E. McCumber, "Effect of ac impedance on dc voltage-current characteristics of superconductor weak-link junction," *J. Appl. Phys.*, vol. 39, pp. 3113–3118, Jun. 1968.

[2] ——, "Tunneling and weak-link superconductor phenomena having potential device applications," *J. Appl. Phys.*, vol. 39, p. 2503, May 1968.

[3] W. C. Stewart, "Current-voltage characteristics of Josephson junction," *Appl. Phys. Lett.*, vol. 12, pp. 277–280, 1968.

[4] T. Van Duzer and C. W. Turner, *Principles of Superconductive Devices and Circuits*, 2nd ed: Prentice-Hall, 1999.

[5] A. B. Kaul, L. Yu, N. Newman, J. M. Rowell, S. R. Whiteley, and T. Van Duzer, "High $I_c R_N$ internally shunted sputtered NbN Josephson junctions with a TaN_x barrier for nonlatching logic applications," *Appl. Phys. Lett.*, vol. 78, pp. 99–102, Jan. 1, 2001.

[6] J. Clarke, "Supercurrents in lead-copper-lead sandwiches," *Proc. Roy. Soc.*, vol. 308, pp. 447–471, 1969.

[7] C. L. Huang and T. Van Duzer, "Single-crystal silicon-barrier Josephson junction," *IEEE Trans. Mag.*, vol. MAG-11, pp. 753–756, Mar. 1975.

[8] A. M. Kadin, C. A. Mancini, M. J. Feldman, and D. K. Brock, "Can RSFQ logic circuit be scaled to deep submicron junctions?," *IEEE Trans. Appl. Superconduct.*, vol. 11, no. 1, pp. 1050–1055, Mar. 2001.

[9] K. K. Likharev, "Superconducting weak links," *Rev. Mod. Phys.*, vol. 51, pp. 101–159, Jan. 1979.

[10] F. Wooten, *Optical Properties of Solids*. New York: Academic, 1972.

[11] T. Van Duzer, L. Zheng, X. Meng, C. Loyo, S. R. Whiteley, L. Yu, N. Newman, J. M. Rowell, and N. Yoshikawa, "Engineering issues in high-frequency RSFQ circuits," *Physica C*, vol. 372–376, pp. 1–6, Aug. 1, 2002.

[12] L. Yu, C. Stampfl, D. Marshall, T. Eshrich, J. M. Rowell, N. Newman, and A. J. Freeman, "Mechanism and control of the metal-to-insulator transition in rocksalt tantalum nitride," *Phys. Rev. B*, vol. 65, p. 245 110, Jun. 2002.

[13] D. R. Heslinga and T. M. Klapwijk, "Schottky barrier and contact resistance at a niobium/silicon interface," *Appl. Phys. Lett.*, vol. 54, pp. 1048–1050, Mar. 1989.

[14] K. A. Delin and A. W. Kleinsasser, "Stationary properties of high-critical-temperature proximity effect Josephson junctions," *Superconduct. Sci. Technol.*, vol. 9, pp. 227–269, 1996.

[15] K. Biedermann, A. Chrestin, T. Matsuyama, and U. Merkt, "Ac Josephson effects in Nb/InAs/Nb junctions with integrated resonators," *Phys. Rev. B*, vol. 63, p. 144 512, 2001.

[16] W. M. van Huffelen, T. M. Klapwijk, D. R. Heslinga, M. J. de Boer, and N. van der Post, "Carrier transport in mesoscopic silicon-coupled superconducting junctions," *Phys. Rev. B*, vol. 47, pp. 5170–5189, Mar. 1993.

[17] T. M. Klapwijk, G. E. Blonder, and M. Tinkham, "Explanation of subharmonic energy gap structure in superconducting contacts," *Physica B & C*, vol. 110, pp. 1657–1664, 1982.

[18] M. Y. Kupriyanov and V. F. Lukichev, "The influence of the proximity effect in the electrodes on the stationary properties of S-N-S Josephson structures," *Sov. J. Low Temp. Phys.*, vol. 8, p. 526, 1982.

[19] I. A. Devyatov and M. Y. Kupriyanov, "Resonant tunneling and long-range proximity effect," *JETP Lett.*, vol. 59, p. 200, 1994.

Lei Yu was born in Shanghai, China, on July 16, 1975. He received the B.A. degree in physics and mathematics from Kenyon College, Gambier, OH, the M.S. degree in electrical engineering from Northwestern University, Evanston, IL, and the Ph.D. degree in electrical engineering from Arizona State University, Tempe, in 2005.

His thesis work and current research involve design, fabrication, characterization, and modeling of SNS Josephson junctions with barrier material tuned near the metal–insulator transition.

Nathan Newman was born in Oakland, CA. He received the M.S. and Ph.D. degrees from Stanford University, Stanford, CA, in 1983 and 1987, respectively. He received the B.S. degree in biomedical/electrical engineering from the University of Southern California, Pasadena, in 1981.

He is currently a Professor in the Chemical and Materials Engineering Department, Arizona State University, Tempe. Since earning his doctorate degree, he has been employed as an Associate Professor at Northwestern University and a member of the technical staff at the University of California at Berkeley, Lawrence Berkeley Laboratory, Stanford University, and Conductus, Inc. His research interests include novel solid-state materials for microwave, photonic, and high-speed applications. His current work involves synthesis, characterization and modeling of III-N semiconductors, high-Q microwave dielectrics, superconductor SNS junctions for 100+ GHz digital logic, heterojunctions, metal/III–V semiconductor interfaces, and nonstoichiometric transition-metal nitrides near the metal–insulator transition.

John M. Rowell received the Ph.D. degree from Oxford University, Oxford, U.K., studying impurity conduction (now known as the metal-insulator transition) in germanium.

He joined Bell Laboratories in 1961. Soon afterwards, with P. W. Anderson, he made the first observation of the Josephson effect and demonstrated the magnetic field sensitivity of thze Josephson current. With W. L. McMillan, he developed tunneling spectroscopy, a measurement technique that determines in detail the electron–phonon interaction that causes superconductivity, at least in the low-Tc materials. In a collaboration with J. Geerk, M. Gurvitch, and M. Washington, he invented the niobium/aluminum Josephson junction process that is now the basis of all low-Tc digital electronics and magnetic sensors. He held a series of management positions at Bell Laboratories and became Director of the Chemical Physics Laboratory in 1981. In 1983, just prior to the divestiture of the Bell System, he joined Bell Communications Research (Bellcore) as Assistant Vice President of Solid State Science and Technology. He was responsible for guiding the growth of this laboratory from its beginning, including both personnel and facilities. The technical programs of the laboratory included materials research, optoelectronics, optical switching, high-speed electronics, and high-Tc superconductivity. He joined Conductus, a startup superconducting electronics company, in 1989, as Chief Technical Officer and served as President of the company for the year of 1991. In 1997, he was appointed as the Materials Institute Professor at Northwestern University and since 2001 has been a Visiting Professor at Arizona State University, Tempe.

Dr. Rowell held the first patent granted for logic applications of the Josephson effect. In 1978, he received the Fritz London Memorial Low Temperature Physics Prize for his work on the Josephson Effect, tunneling, and superconductivity. He is a Fellow of the American Physical Society and in 1989 was elected a Fellow of the Royal Society. He became a member of the National Academy of Sciences, in 1994, and of the National Academy of Engineering, in 1995.

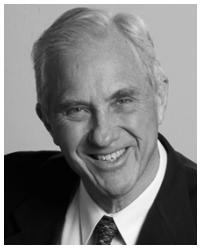

Theodore Van Duzer (S'52–A'54–M'60–SM'75–F'77–LF'93) received the B.S. degree in electrical engineering from Rutgers University, New Brunswick, NJ, the M.S. degree in engineering from the University of California, Los Angeles, and the Ph.D. degree in electrical engineering from the University of California, Berkeley, in 1960.

He has been on the faculty of Electrical Engineering and Computer Sciences at the University of California, Berkeley, since 1961 and is currently a Professor in the Graduate School. He has led a research group in superconductive electronics since 1968, including both devices and circuits. He and members of his group invented a Josephson junction with electron-pair coupling through a 500-angstrom-thick degenerately doped silicon barrier and a planar equivalent and demonstrated both voltage-state and single-flux-quantum digital circuits operating in the high multigigahertz range. His present research is focused on hybrid superconductor/semiconductor systems for cryogenic memory. In 1988, he helped form the company Conductus, Inc., to exploit high-temperature superconductors. He has published over 230 technical papers in the field, mostly focused on superconductor device and circuit technology.

Dr. Van Duzer has served on the boards of several continuing international and domestic conferences and workshops on superconductive electronics. He initiated and served as the founding Editor-in-Chief for the IEEE TRANSACTIONS ON SUPERCONDUCTIVITY as well as Guest Editor for several IEEE journal special issues. He is coauthor (with S. Ramo and J. R. Whinnery) of *Fields and Waves in Communication Electronics* (50th anniversary edition) and coauthor (with C. W. Turner) of *Introduction to Superconductive Devices and Circuits* (2nd ed., 1999), which appeared in English, Russian, Japanese, and Chinese. He is a member of the U.S. National Academy of Engineering.